“© 2021 IEEE. Personal use of this material is permitted. Permission from IEEE must be obtained for all other uses, in any current or future media, including reprinting/republishing this material for advertising or promotional purposes, creating new collective works, for resale or redistribution to servers or lists, or reuse of any copyrighted component of this work in other works.”

A Quantitative Approach for Convergence Analysis of a Singularly Perturbed Inverter-Based Microgrid

Abhishek Nayak, Madan Mohan Rayguru, Sukumar Mishra, *Senior Member, IEEE* and M. J. Hossain, *Senior Member, IEEE*

***Abstract*—A reduced-order model of a converter-dominated microgrid system may not resemble its full-order system associated with uncertainties. This paper aims to provide a singular perturbation-based contraction framework for model order reduction in converter-dominated uncertain microgrid systems. For this purpose, the concerned microgrid system is modeled as a generalized multi-timescale system, and certain sufficient conditions are derived such that convergence between the trajectories of the uncertain full-order and the corresponding reduced-order model can be guaranteed. The contraction theory-based strategy also provides explicit parameter-dependent expressions for quantifying discrepancies. The derived results are utilized to analyze the inverter-based microgrid system's convergence behavior and obtain uncertainty bounds on its parameters. Further, the effects of modeling uncertainties and different loading conditions on the reduced-order model's validity are also discussed. It is observed that for any uncertainty associated with the microgrid parameters that are within the bounds of checkable conditions, the states of the reduced-order microgrid model converge to that of the uncertain full-order system. Further, it is also shown that the obtained discrepancy expressions are more precise than state of the art.**

***Index Terms*—Contraction, Partial contraction, timescale, microgrid system, multi-microgrid system.**

I. Introduction

LARGE installations of distributed generators (DGs) have increased significantly in recent years to harness clean energy and reduce greenhouse gas emissions. Such scattered DGs have been looked upon for clustering to form a multi-microgrid (MMG) system [1], [2]. An MMG system forms a building block for future smart grids and provides an excellent opportunity to manage large-scale DGs' operations with composite dynamic behaviors. The power flow interactions between the small-size large-scale inverter-based microgrids (IBMGs) introduce increased complexity for analyzing a high-dimensional MMG system. A reduced-order model of an IBMG system obtained by preserving the power control loop states and discarding the myriad ones can provide a convenient and feasible way to analyze the power flow behavior and design secondary and tertiary controllers [3]–[10].

Model order reduction techniques for large-scale systems can be broadly divided into different mathematical methods based on polynomial approximation, optimization, singular perturbation, balanced truncation, Hankel norm approximation, etc. [11]–[14]. However, there is no universal model order reduction method that suits all purposes and all classes of real-world systems. Thus, the choice of a particular technique depends on the application domain and operating conditions [12], [15], [16]. For example, it was found that the singular perturbation (SP) technique can be a suitable choice for low-frequency operation, whereas balanced truncation may be a better option in high-frequency applications [12], [16]. The SP-based model reduction can preserve the physical realization, which means that the internal state variables of the reduced-order system correspond to the actual system state trajectories [12]. Further, the SP-based model order reduction uses the physical properties of a large system that often exists in multiple timescales; this means the system's internal state variables evolve at different speeds.

A system with multiple timescales is conveniently represented by a singularly perturbed system (SPS) form of representation [17]. In an SPS form of representation, the fast-evolving states are represented by multiplying their derivatives with singular perturbation parameters (SPP or ε). The SPP is generally modeled from the time constant of the fast dynamics, and the reduced-order model is obtained by suppressing the SPP ($\varepsilon \to 0$) such that the fast dynamics are reduced to an algebraic equation. The root of the algebraic equation is commonly referred to as the slow manifold. The obtained reduced-order model can approximate the corresponding full-order model if the fast states converge to the slow manifold and the SPP is sufficiently small. Conventionally, techniques such as Lyapunov stability analysis and Tikhonov's theorem have been used to obtain the bound on the SPP (ε^*) [10], [15]–[18]. However, with these approaches, the derived discrepancy expressions between the full-order system and the reduced-order model are independent of the SPP. In other words, one cannot quantify the discrepancy behavior between the reduced-order model and full-order system when the SPP is varying within the obtained bound ($\varepsilon \leq \varepsilon^*$). Recently, in [19]–[22] contraction theory was explored to not only obtain the bound on the SPP but also express the discrepancy in terms of SPP. The main limitation of the approach followed in [19]–[22] is that it requires the evolution of the slow manifold to be upper bounded by a constant. As the slow manifold dynamics depends on the states, this condition may restrict the states to only evolve inside certain bounded regions and will result in a conservative discrepancy expression.

The SP-based model order reduction techniques have been utilized for the analysis of islanded IBMG systems [7]–[10]. So far in the literature, SP-based model reduction for IBMGs has focused either on exploiting the technique to obtain a simpler mathematical model for time/frequency domain analysis or using the obtained reduced-order models for controller design (secondary/tertiary). However, in a practical scenario,

A. Nayak and S. Mishra are with the Department of Electrical Engineering, Indian Institute of Technology, Delhi, New Delhi, 110016 India.

M. M. Rayguru is with the Engineering Product Development Pillar, Singapore University of Technology Design, Singapore.

M. J. Hossain is with the School of Electrical and Data Engineering, University of Technology, Sydney, Australia.

IBMGs may be affected by external disturbances, parameter uncertainties, and modeling errors. Thus, any analysis or controller design based on the reduced-order model obtained from a nominal full-order system ~~may~~ produce erroneous results when implemented in an actual uncertain system. This argument signifies the importance of investigating the bounds on external disturbances and parameter fluctuations under which the reduced-order model can be ~~said~~ to be valid.

To address the above limitations in discrepancy measures of model-order reduction techniques and provide a quantitative framework for the model-order reduction of an IBMG system, this paper proposes a generalized contraction theory-based setup for analyzing the convergence behavior of a reduced-order IBMG model with an uncertain full-order system. The main contributions of the paper are to:

(i) Analyze different time-scales present in an IBMG system and provide an improved model order reduction algorithm based on the SP method. Further, appropriate mapping terms are provided to facilitate the interconnections between the reduced-order IBMG models in an MMG environment.

(ii) Provide a generalized contraction theory-based framework for SP-based model order reduction in an uncertain multi-timescale system. The framework derives certain checkable conditions based on the norm of uncertainties to examine the reduced-order model's validity. Further, explicit expressions for discrepancies in the state trajectories are provided in terms of SPP.

(iii) Implement and validate the proposed quantitative framework for the model order reduction of an uncertain IBMG system for different scenarios such as parameter uncertainties, modeling errors, shifts in operating points and exogenous signals arising from the cross-coupling effect.

The paper is organized as follows: Section II presents the IBMG's timescales, model reduction, and mapping expressions for realizing an MMG system. Section III provides the quantitative bound for the SPP under systems' parametric and modeling uncertainties. Section IV presents the convergence analysis in the IBMG system under various case studies. Finally, in Section V, conclusions are drawn.

II. Model Order Reduction of an IBMG System in an MMG Environment

In a typical MMG system, as shown in Fig.1, each IBMG can either operate autonomously under grid fault conditions or can exchange power with other IBMGs through an external network to form a reliable power network [1], [2]. Each IBMG as shown in Fig.1 constitutes multiple states, and when these IBMGs are interconnected to form an MMG system, the resultant system becomes a huge dynamical system. A reduced-order model of such an MMG system will assist in simplifying analysis and design. One approach is to reduce the MMG system as a whole. However, with this approach, one has to obtain the reduced-order model of the MMG each time an IBMG is connected or disconnected. Another approach is to obtain reduced-order model of each IBMG and interconnect them through appropriate mapping expression. With the latter approach, the advantages of modularity and scalability are achieved. In this regard, first, a model order reduction methodology for an IBMG is discussed, then the mapping expressions for interconnecting the reduced-order models of IBMGs are discussed.

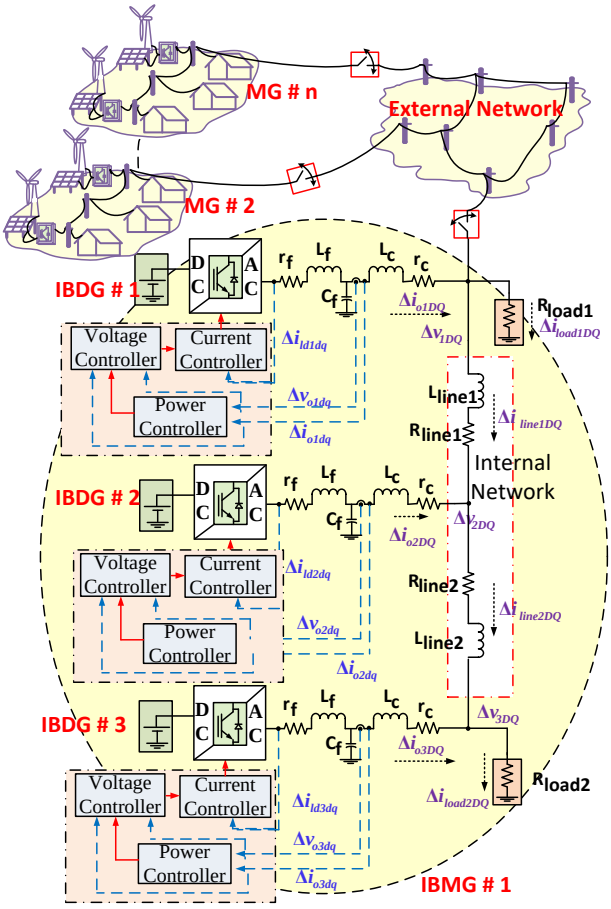

Fig. 1. Schematic diagram of a multimicrogrid (MMG) system.

A. System Description of an IBMG

In Fig.1, the IBMG#1 represents the islanded microgrid system whose dynamic model has been discussed in [23]. The IBMG#1 consists of three inverter-based distributed generators (IBDGs) and an internal network with two power lines. The dynamics of the IBMG#1 system can be given as:

$$\dot{X}_{mg} = A_{mg} X_{mg} \tag{1}$$

where $X_{mg} = [\Delta x_{inv1}, \Delta x_{inv2}, \Delta x_{inv3}, \Delta i_{lineDQ\ 1}, \Delta i_{lineDQ\ 2}]^T$ represents the associated states, and the state matrix A_{mg} is given as (2):

$$A_{mg} = \begin{bmatrix} A_{I_1} & [0] & [0] & B_{I_1L_1} & [0] \\ B_{I_2I_1} & A_{I_2} & [0] & B_{I_2L_1} & B_{I_2L_2} \\ B_{I_3I_1} & [0] & A_{I_3} & [0] & B_{I_3L_2} \\ \begin{bmatrix} B_{L_1I_1} + \\ B_{L_1I_{1_0}} \end{bmatrix} & B_{L_1I_2} & [0] & A_{L_1} & B_{L_1L_2} \\ B_{L_2I_{1_0}} & B_{L_2I_2} & B_{L_2I_3} & B_{L_2L_1} & A_{L_2} \end{bmatrix} \tag{2}$$

The A_{mg} matrix has been defined in Appendix A.

The states of an i^{th} inverter are given as

$$x_{inv\ i} = [\Delta\delta_i, \Delta P_i, \Delta Q_i, \Delta\phi_{di}, \Delta\phi_{qi}, \Delta\gamma_{di}, \Delta\gamma_{qi}, \Delta i_{ldi}, \Delta i_{lqi}, \Delta v_{odi}, \Delta v_{oqi}, \Delta i_{odi}, \Delta i_{oqi}]^T \tag{3}$$

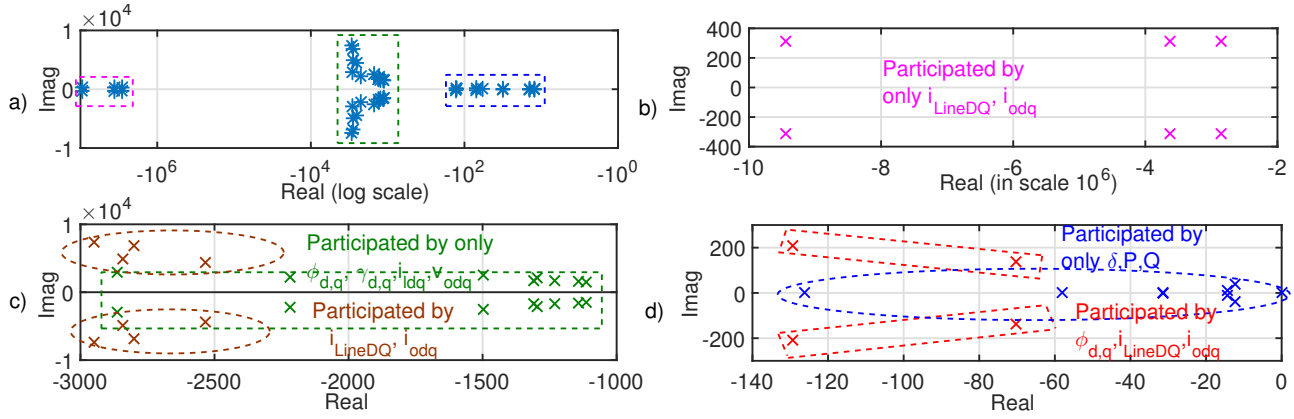

Fig. 2. Eigenvalue plot for the IBMG1 a) Eigenvalue of IBMG1 showing multiple time scales b) Eigenvalue in the range of -10^6 to -2^6 c) Eigenvalue in the range of -3000 to -1000 and d) Eigenvalue in the range of -120 to 0.

where $\Delta\delta_i$ represents the angle between an individual inverter reference frame with its common reference frame, ΔP_i and ΔQ_i represent filtered real and reactive power states respectively, $\Delta\phi_{di}$ and $\Delta\phi_{qi}$ represent the states of the voltage controller, and $\Delta\gamma_{di}$ and $\Delta\gamma_{qi}$ represent the states of the current controller. The states $\Delta i_{ldqi}, \Delta v_{odqi}, \Delta i_{odqi}$ represent the output LC filter inductance current, capacitance voltage and coupling inductance current respectively. The states $i_{lineDQj} = [i_{lineDj}, i_{lineQj}]^T$ represent the direct and quadrature axis line current of the j^{th} line. The load dynamics are neglected in the analysis by considering resistive loads for simplicity.

The dynamics of IBMG#1 (1) consists of 43 states (13 states of each inverter and two states of each power line) and can be examined for possible order reduction by using the singular perturbation-based technique.

B. Timescale Separations and SPS Form of IBMG

A system involving multiple timescale dynamics ~~may~~ be suitably represented in SPS form [17]. One of the convenient approaches for visualizing multiple timescales involved in a system is through the plotting of eigenvalues. A system with eigenvalues in different clusters represents different timescales involved in that system [18]. The eigenvalues of the IBMG system (1) are plotted in Fig.2 and can be seen to exist in three different clusters (timescale). The participation of the states in these modes differentiates their timescale behavior.

Fig.2 shows that the states Δi_{lineDQ} and Δi_{odq} participate with the modes present in the region -10×10^6 to -2×10^6 of the real axis. The states $\Delta\phi_{dq}, \Delta\gamma_{dq}, \Delta i_{ldq}, \Delta v_{odq}$ participate with the modes present in the region -3000 to -2000 of the real axis. It can be observed that some modes in this timescale also participate in the network dynamics states (Δi_{lineDQ} and Δi_{odq}). One can observe that the high frequency components in the eigenvalues shown in Fig.2(b) are filtered out by the capacitor filter (C_f) in Fig.2(c). The states participating with the modes in the region -120 to 0 of the real axis are from the inverters' power control loops. It can also be observed that four modes in this timescale participate in the states of current loop, internal network and coupling inductance ($\Delta\phi, \Delta i_{lineDQ}$ and i_{odq}). This participation of Δi_{lineDQ} and i_{odq} in the slow modes shows the existence of cross-coupling terms and can be verified from the expressions in Appendix A. From the above observation on the eigenvalues clusters, it can be said that the IBMG system (1) exhibits three timescale behaviors.

TABLE I
PARAMETERS THAT DEFINE SPP

ε	Expression	Nominal value (P_0)
ε_2	$max\{\frac{L_{line_1}}{2r_n}, \frac{L_{line_2}}{2r_n}, \frac{L_c}{r_n}\}$	$max\{\{1.59, 9.23, 3.5\}\times10^{-7}\}$
ε_1	$max\{\frac{L_f}{K_{pc}^2}, \frac{1}{K_{iv}}, C_f\}$	$max\{\{0.122, 26, 0.5\}\times10^{-4}\}$

The above analysis through the participation factor can also be verified from the IBMG dynamics given by the first principle (2). The power network dynamics and coupling inductors are observed to be scaled by the time constant $\frac{L_{line}}{2r_n}$ and $\frac{L_C}{r_{LC}+r_n}$, respectively, whose values lie in the range 10^{-6}. Similarly, the time constant for the *LCL* filters ($\frac{L_f}{r_f+K_{pc}}$) and the power control loop ($\frac{1}{\omega_c}$) lie in the range of 10^{-3} and 10^{-1}, respectively. From the above two different analyses, it can be concluded that the IBMG dynamics exist in three timescales. Based on the above analysis, the microgrid dynamics (1) can be rewritten in three timescale SPS forms as:

$$\begin{bmatrix} \Delta\dot{x} \\ \varepsilon_1\Delta\dot{z}_1 \\ \varepsilon_2\Delta\dot{z}_2 \end{bmatrix} = \begin{bmatrix} \varphi_{11} & \varphi_{12} & \varphi_{13} \\ \varphi_{21} & \varphi_{22} & \varphi_{23} \\ \varphi_{31} & \varphi_{32} & \varphi_{33} \end{bmatrix} \begin{bmatrix} \Delta x \\ \Delta z_1 \\ \Delta z_2 \end{bmatrix} = [\Phi] \begin{bmatrix} \Delta x \\ \Delta z_1 \\ \Delta z_2 \end{bmatrix} \tag{4}$$

where the $\varepsilon_{1,2}$ are the SPPs, whose values are presented in Table I. The states are categorized into different groups depending upon their rate of evolution in the microgrid dynamics, which are $x = \{\Delta\delta_i, \Delta P_i, \Delta Q_i \Delta\phi_{dqi}\}$, $\Delta z_1 = \{\Delta\gamma_{dqi}, \Delta i_{ldqi}, \Delta v_{odqi}\}$ and $\Delta z_2 = \{\Delta i_{odqi}, \Delta i_{lineDQj}\}$ for $i \in \{1,2,3\}$ and $j \in \{1,2\}$. The state matrix 'Φ' is obtained after appropriate transformation as $\Phi = Ep(TA_{mg}T^{-1})$, where 'T' is a matrix that rearranges the rows of the A_{mg} in (1), and the 'Ep' is a diagonal matrix consisting of SPPs ($diag(1, \varepsilon_1, \varepsilon_2)$).

The obtained IBMG dynamics in SPS (4) may be used for model order reduction by following the SP technique [17]. However, the SP technique for model order reduction is given for a standard two-timescale system. Systems such as (4) with multiple timescales can be iteratively reduced to a lower order

Algorithm 1 Multi-Timescale Model Order Reduction

1: # Given a multi-timescale system represented as (5):

$$\begin{aligned} \dot{x} &= f(x, z_1, .., z_r, z_{r+1}, .., z_n) \\ \varepsilon_1 \dot{z}_1 &= g_1(x, z_1, .., z_r, z_{r+1}, .., z_n, \varepsilon_1) \\ &\cdot \\ \varepsilon_n \dot{z}_n &= g_n(x, z_1, .., z_r, z_{r+1}, .., z_n, \varepsilon_n) \end{aligned} \tag{5}$$

2: # Create a function matrix FG from (5) as:

$$FG = [f, g_1, .., g_n]^T \tag{6}$$

3: # Start running the loop for the order reduction of (5):
for $i = n : -1 : 1$

4: # Separate the states and the function matrix FG in (5) to a two-timescale form as:

$$X_i = [x, z_1, .., z_{i-1}]^T; \; Z_i = [z_i] \tag{7}$$

$$F_i(X_i, Z_i, t) = [I_{i\times i}, [0]_{i\times 1}] \times FG \tag{8}$$

$$G_i(X_i, Z_i, \varepsilon_i) = [[0]_{1\times i}, 1] \times FG \tag{9}$$

where I and $[0]$ represent the identity matrix and zero vector of appropriate dimensions, respectively.

5: # Reformulate (5) in two-timescale form as (10):

$$\dot{X}_i = F_i(X_i, Z_i, t) \tag{10}$$

$$\varepsilon_i \dot{Z}_i = G_i(X_i, Z_i, \varepsilon_i) \tag{11}$$

6: # Suppress the SPP($\varepsilon_i \to 0$) and obtain the algebraic expression ($\vartheta_i(X_i)$) for Z_i dynamics :

$$G_i(X_i, Z_i) = 0; \; \vartheta_i(X_i) = Z_i \tag{12}$$

7: # Obtain the reduced-order model of (10) in terms of X_i:

$$\dot{x}_{red\ i} = F_i(X_i, \vartheta_i(X_i), t) \tag{13}$$

8: # Update the nonlinear function matrix FG:

$$FG = [F_i] \tag{14}$$

9: # Repeat the loop to obtain the final reduced-order model:
end for

by converting the multiple-timescale system to two timescales for each ε as shown in Algorithm 1.

C. IBMG Model Order Reduction

The multi-timescale IBMG model (4) is reduced to power control loop states by following Algorithm 1 and letting the resultant reduced-order model be represented as:

$$\dot{x}_{red} = A_{red} x_{red} \tag{15}$$

where $x_{red} = \{\Delta\delta_i, \Delta P_i, \Delta Q_i, \Delta\phi_{dqi}\}$ and A_{red} are the states and state matrix of the reduced-order model respectively. The states trajectories of the full-order system and reduced-order

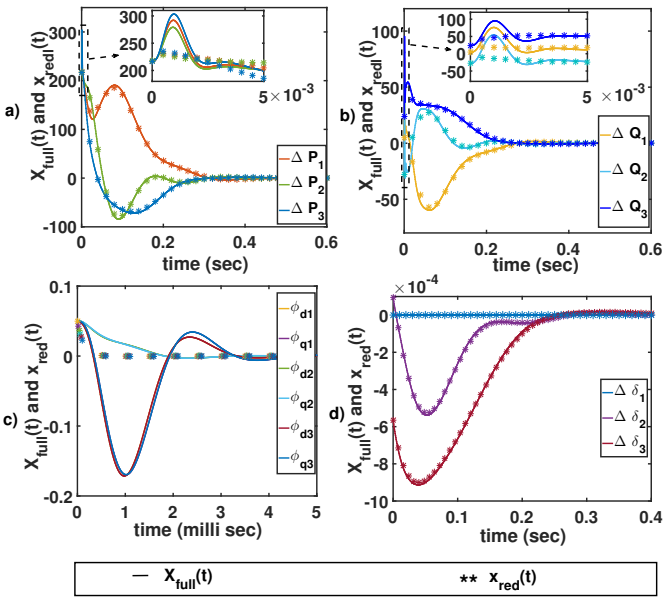

Fig. 3. Reduced order and corresponding full order system state trajectories for a) $\Delta P, \Delta Q$ and b) $\Delta\delta$ and $\Delta\phi$ for all inverters.

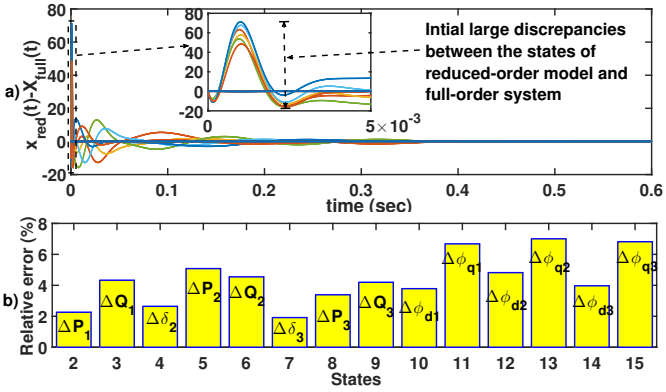

Fig. 4. a) States trajectories error between full- and reduced-order models b) percentage relative error between the states after $t \geq 3msec$.

model are shown in Fig.3 by considering the initial conditions of the states as 5% of the IBMG operating condition.

An interesting observation can be made from Fig.4(a) that the initial discrepancy between the states of the reduced-order model and the full-order system is high during the period $t \leq 0.0026$ seconds (from Table I it can be seen that the timescale separation is given by $\varepsilon_1 = 0.0026$). This can be explained as the $x_{red}(t)$ dynamics contains the algebraic solution of $Z(t)$ dynamics in the form of $\vartheta(x(t))$, whereas in the full-order system the dynamics of $Z(t)$ influence the solution of $x(t)$. However, after the initial large discrepancy, the state trajectories of the reduced-order model and full-order model follow each other. The relative error is calculated as $||X(t) - x_{red}(t)||/||X(t)||$, and is plotted in Fig.4(b) for $t \geq 0.003$ seconds. It can be observed that the relative error is within 7%, and the reduced-order model can be used for various analysis and design purposes.

D. Mapping Between Reduced-Order Models of IBMGs

When multiple IBMGs are interconnected to form an MMG system, the internal network power lines of an IBMG exchange currents with that of the external network. However, in the reduced-order model for an IBMG obtained in (15), the states of the internal network dynamics are not present. Under such a scenario, the model order reduction based on the SP method is required to be carried out while incorporating external network dynamics as coupling inputs. The resultant reduced-order model will have mapping terms between the reduced-order models of IBMGs.

Let the dynamics for an MMG system consist of 'n' number of IBMGs and 'm' number of lines in the external network. For simplicity, let us consider each IBMG as consisting of 'n_i' number of IBDGs and 'n_n' number of internal network lines. The dynamics of such an MMG system is given as:

$$\begin{aligned}\dot{X}_{MG_i} =&[A_{MG_i}]_{((13n_i+2n_n)\times(13n_i+2n_n))}X_{MG_i}\\ &+[B_{MG_iExN}]_{((13n_i+2n_n)\times 2m)}x_{ExN}\\ &+[B_{MG_i\omega_{com}}]_{((13n_i+2n_n)\times(13n_i+2n_n))}X_{MG_1}\\ \dot{x}_{ExN} =&[A_{ExN}]_{(2m\times 2m)}x_{ExN}+\sum_{i=1}^{n}[B_{ExNMG_i}]_{(2m\times(13n_i+2n_n))}X_{MG_i}\end{aligned} \tag{16}$$

where x_{MG_i}, A_{MG_i}, B_{MG_iExN} and $B_{MG_i\omega_{com}}$ are the states, state matrix, coupling matrix to external network and coupling matrix to reference IBMG (for common reference) respectively. The *IBMG*#1 is considered to include the reference IBDG for the whole MMG system.

Like the internal network dynamics, the external network dynamics also lies in a fast timescale with respect to the power control loop states. The complete MMG system (16) can be represented in SPS form as given in expression (17) (similar to the procedure followed for (4)). The reduced-order model for the IBMG system can be obtained by following Algorithm 1 ($\varepsilon \to 0$), and the external network dynamics that interconnect different IBMGs can be reduced to an algebraic expression by suppressing its SPP ($\varepsilon_{ExN} \to 0$). The reduced-order differential-algebraic model of an MMG system is given as:

$$\begin{aligned}\dot{x}_{MGred_i} =&[A_{MGred_i}]_{(5n_i\times 5n_i)}x_{MGred_i}-[B_{MG_iExNred}]_{(5n_i\times 2m)}x_{ExN}\\ &+[B_{MGred_i\omega_{com}}]_{(5n_i\times 5n_i)}x_{MGred_1}\\ x_{ExN} =&-[A_{ExNred}]^{-1}_{(2m\times 2m)}[B_{ExNMGred}]_{(2m\times 5n_in)}\begin{bmatrix}x_{MGred_1}\\ \cdot\\ x_{MGred_n}\end{bmatrix}\end{aligned} \tag{18}$$

where x_{MGred_i} and A_{MGred_i} are the reduced-order model of i^{th} IBMG states in terms of the power control loop and state matrix, respectively. The matrix $[B_{MG_iExNred}]$ and $[A_{ExNred}]^{-1}[B_{ExNMGred}]$ form the mapping matrix between the IBMGs. All the involved terms in the expressions are provided in Appendix B.

It can be observed from (16) and (18) that the full-order MMG system of order '$13n_in+2n_nn+2m$' is reduced to '$5n_in$'. Further, it should be noted that the reduced-order model state matrix 'A_{MGred_i}' for an IBMG is the same as the state matrix obtained earlier in (15), and the mapping between the $IBMG_i$ with the other IBMGs are given through the matrix $[B_{MG_iExNred}][A_{ExNred}]^{-1}[B_{ExNMGred}]$.

E. Discrepancy between Reduced-Order and Full-Order IBMG Models under Uncertainties

Fig.4(a) shows the discrepancies between the states for the reduced-order model and full-order system with nominal parameters. However, the parameters of the microgrid (1) may vary due to uncertainties in environmental conditions, human factors or ageing. Under these cases, there will be an increase in discrepancies between the uncertain full-order system and the reduced-order model compared with the one shown in Fig.4(a). A case study on the behavior of such discrepancies is illustrated in Fig.5 for variations in the parameters of L_f. It can be observed that the discrepancy increases with the increase in parameters variations from its nominal value, and after a certain limit it explodes.

The reduced-order models obtained from other model-order reduction techniques such as Hankel model reduction or balanced stochastic model truncation will also experience such an increase in discrepancy behavior as shown in Fig.6. In these model-order reduction techniques, the criteria for model-order reduction is to measure the full-order system's states energy, and in the reduce-order model the high energy states are retained by discarding the low energy ones [24], [25]. In these techniques, it is difficult to establish a direct relationship between the parameter variation in an uncertain system and the discrepancy between the reduced-order model and uncertain full-order system. In the SP-based model order reduction, the reduced-order model is obtained by considering the different timescales present in a system, where the fast state dynamics are discarded, and the slow ones are retained. These systems can be represented in SPS form as represented in (4) and (17), where the SPP models the timescale separation. In this case, there is a direct relationship between the model reduction criteria ($\varepsilon \to 0$) and the system parameters. Thus, the effect of

$$\begin{aligned}\dot{x}_{MG_i} =&[\varphi_{MG_i(1,1)}]_{(5n_i\times 5n_i)}x_{MG_i}+[\varphi_{MG_i(1,2)}]_{(5n_i\times(8n_i+2n_n))}z_{MG_i}+[\psi_{MG_iExN(1)}]_{(5n_i\times 2m)}x_{ExN}+[\psi_{MG_i\omega_{com}(1)}]_{(5n_i\times 5n_i)}x_{MG_1}\\ \varepsilon\dot{z}_{MG_i} =&[\varphi_{MG_i(2,1)}]_{((8n_i+2n_n)\times 5n_i)}x_{MG_i}+[\varphi_{MG_i(2,2)}]_{((8n_i+2n_n)\times(8n_i+2n_n))}z_{MG_i}+[\psi_{MG_iExN(2)}]_{((8n_i+2n_n)\times 2m)}x_{ExN}\\ &+[\psi_{MG_i\omega_{com}(2)}]_{((8n_i+2n_n)\times 5n_i)}x_{MG_1}\\ \varepsilon_{ExN}\dot{x}_{ExN} =&[\varphi_{ExN}]_{(2m\times 2m)}x_{ExN}+\sum_{i=1}^{n}\begin{bmatrix}[\psi_{ExNMG_i(1)}]_{(2m\times 5n_i)} & [\psi_{ExNMG_i(2)}]_{(2m\times(8n_i+2n_n))}\end{bmatrix}\begin{bmatrix}x_{MG_i}\\ z_{MG_i}\end{bmatrix}_{((13n+2n_n)\times 1)}\end{aligned} \tag{17}$$

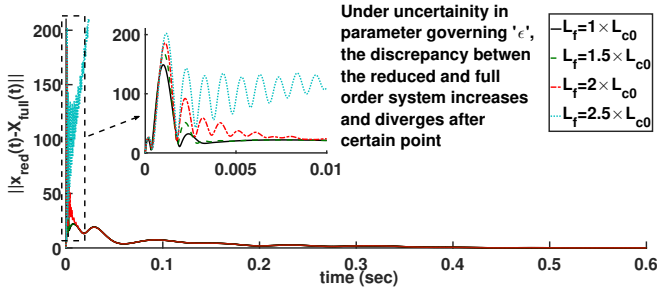

Fig. 5. Effect of uncertainty in the L_f parameter of IBMG on the discrepancy between the reduced-order model and the full-order system.

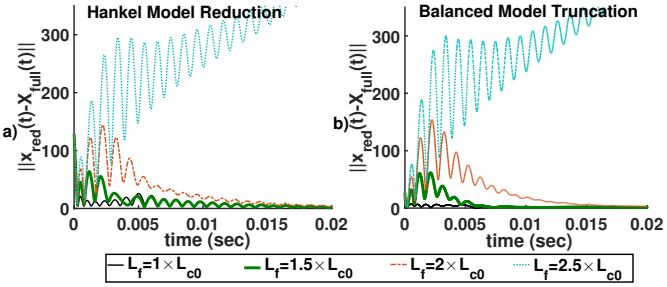

Fig. 6. Effect of uncertainty in L_f parameter of IBMG on the discrepancy between the reduced-order model and the full-order system a) Reduced-order model obtained using Hankel model reduction b) Reduced-order model obtained using Balanced stochastic model truncation.

variations in system parameters on the discrepancy between the reduced-order model and full-order system can be established through an expression. This forms the motivation in this paper for investigating SP-based order reduction in forming a quantitative framework. In the previous documented works on this aspect, the approach had some conservative bounds and provided some limited results on the effect of modeling uncertainties [19]–[22]. The following section discusses these limitations and provides new generalized theoretical results.

III. SPS and its Quantitative Analysis

This section provides a contraction-based convergence analysis for the general class of SPS, which is later utilized to analyze the impact of uncertainties on the model order reduction of uncertain IBMG.

A. Description of SPS

Let the simplified representation for the standard two-timescale system (10) be given as:

$$\begin{aligned} \dot{x} &= f(x,z,t) \\ \varepsilon \dot{z} &= g(x,z,\varepsilon) \end{aligned} \tag{19}$$

where $\varepsilon \in (0,1)$ is a small real number, x is a vector of slow state variables, z is a vector of fast state variables (the state z evolves with respect to t/ε). The terms f and g are nonlinear functions that govern the dynamics of the system (19).

As explained earlier, if the equation $g(z,x)$=0 in (19) has a unique root $z = \vartheta(x)$ (also called slow manifold), then the overall system (19) can be degenerated into a lower order system by suppressing the SPP ($\varepsilon \to 0$).

Let the reduced slow dynamics be given as:

$$\dot{x}_{red} = f(x_{red}, \vartheta(x_{red}), t) \tag{20}$$

where x_{red} represents the states of the reduced-order model. It should be noted that the state variable $x(t)$ in the full-order system (19) and $x_{red}(t)$ in the reduced-order model (20) represent the same state variables in the two different models.

Let us consider $y = z - \vartheta$ (for notational simplicity ϑ represents $\vartheta(x)$ for the rest of the paper); where y represents the discrepancy between the state z and the slow manifold ϑ. In other words, $\dot{y}$ (referred to as boundary layer dynamics) captures the dynamics for the transition from z state to ϑ variable and can be written as:

$$\varepsilon \dot{y} = g(x, y+\vartheta, \varepsilon) - \varepsilon \frac{\partial \vartheta}{\partial x} f(x,z,t) \tag{21}$$

It should be noted that the state $x(t)$ in (19) evolves in a slow timescale, whereas the boundary layer dynamics (21) evolves in a fast timescale.

The SP-based model order reduction exploits the limit $\varepsilon \to 0$ and stability of boundary layer dynamics (21) to approximate the states x of (19) as x_{red} of (20). The subsequent parts of this section will explicitly derive the convergence between the pairs (x, x_{red}) and (z, ϑ) respectively, both in the presence and absence of uncertainties in the system (19). As contraction theory is used as the main tool for these derivations, certain definitions are presented for the ease of readability.

B. Contraction and Partial Contraction

Definition 3.1 (Contraction): A sufficiently smooth dynamical system $\dot{x} = f(x,t)$ is contracting if any pair of trajectories $(x_1(t), x_2(t))$ exponentially converge towards each other, starting from arbitrary initial conditions [26]. The contraction region is defined as the part of state space, inside which the inequality $(\dot{\Theta} + \Theta \frac{\partial f}{\partial x})\Theta^{-1} + ((\dot{\Theta} + \Theta \frac{\partial f}{\partial x})\Theta^{-1})^T \leq -2\lambda I$ holds true for a non-singular matrix Θ (also called associated metric transformation) and a positive constant λ (also called the contraction rate) [22].

Definition 3.2 (Partial Contraction): A system $\dot{x} = f(x,y,t)$ is referred to as partially contracting in x, if a virtual/auxiliary system defined by $\dot{z} = f(z,y,t)$ is contracting in z for any value of $y, \forall t > 0$ [19], [27].

Due to the exponentially convergent nature of trajectories in a contracting/partially contracting system, the corresponding systems are robust to norm bounded and finite gain-type uncertainties [26], [28], [29]. The analysis carried out in the following subsections is built upon these robustness properties.

C. Convergence Analysis of SPS

Consider the boundary layer dynamics (21). For an ideal case, it can be assumed that during the evolution of $y(t)$ the state $x(t)$ is frozen ($\dot{x} = 0$). This case represents the nominal boundary layer dynamics of (21) and can be given as:

$$\varepsilon \dot{y_n} = g(x, y_n + \vartheta, \varepsilon) \tag{22}$$

The discrepancy between the $y(t)$ and $y_n(t)$ i.e $y(t) - y_n(t)$, is governed by the term $-\varepsilon \frac{\partial \vartheta}{\partial x} f(x,z,t)$, which can also be seen as a perturbation term to nominal boundary layer dynamics.

In [19]–[22], the concept of contraction and partial contraction theory have been explored to observe the convergence between $y(t)$ (21) and $y_n(t)$ (22). It has been shown that convergence is possible if the expressions (22) contract in $y(t)$ for any $x(t)$, with a metric Θ_z and a rate $\frac{\lambda_z}{\varepsilon}$. In these approaches, the bound considered on the perturbation term is given as $||\frac{\partial \vartheta}{\partial x} f(x,z)|| \leq d$, where d is a real number or constant. However, it can be observed that the perturbation term $\frac{\partial \vartheta_x}{\partial x} f(x,z)$ is a function of states $x(t)$ and $z(t)$. By bounding the perturbation term through a constant, the impact of state evolution on the boundary layer dynamics is not reflected.

In this paper, the bounds on the perturbation term $(\frac{\partial \vartheta}{\partial x} f(x,z))$ have been reexamined. The basic idea is to exploit the timescale involved in (19) to obtain the bound on $\frac{\partial \vartheta}{\partial x} f(x,z)$. It can be observed that the $z(t)$ evolves in the same timescale as $y(t)$, whereas the $x(t)$ is in a freeze state. With this idea, the evolution of $\vartheta(x(t))$ can be written as:

$$\frac{\partial \vartheta}{\partial x} f(x,z,t) = \frac{\partial \vartheta}{\partial x} f(x,\vartheta,t) + \frac{\partial \vartheta}{\partial x}(f(x,z,t) - f(x,\vartheta,t)). \tag{23}$$

The term $\frac{\partial \vartheta}{\partial x} f(x,\vartheta,t)$ involves only the $x(t)$ state variable, thus it evolves slower compared to the fast variable $y(t)$ and therefore can be represented by a constant. After simple manipulation and exploitation of the Lipschitz property (25), the bound on the perturbation term is given as:

$$||\frac{\partial \vartheta}{\partial x} f(x,z,t)|| \leq c_1 + c_2||z-\vartheta|| = c_1 + c_2||y|| \tag{24}$$

where $c_1, c_2 \in R^+$ and the Lipschitz inequality with α_1 as a Lipschitz constant is given as:

$$||f(x,z,t) - f(x,\vartheta,t)|| \leq \alpha_1||z-\vartheta||. \tag{25}$$

For the obtained bounding condition (24), the following *Lemma* may be given as:

Lemma 3.1: Let the unperturbed nominal dynamics of (21) be partially contracting in $y(t)$ with a transformation metric Θ_z and a rate $\frac{\lambda_z}{\varepsilon}$. Suppose y_0 is the forward bounded solution of the unperturbed nominal dynamics (22) inside the region of interest such that $||y_n(t)|| \leq y_o$, $\forall t \geq 0$. If the perturbation term satisfies (24) and $\varepsilon \leq \frac{\lambda_z}{\chi_z c_2}$, where χ_z is condition number of Θ_z, then the discrepancy between the boundary layer trajectories $y(t)$ and the nominal trajectories $y_n(t)$ can be quantified as (26):

$$||y(t) - y_n(t)|| \leq \chi_z e^{(-\frac{\lambda_z - \varepsilon c_2 \chi_z}{\varepsilon})t}||y(0) - y_n(0)|| + \frac{(c_1 + c_2 y_o)\chi_z}{\lambda_z - \varepsilon c_2 \chi_z}\varepsilon. \tag{26}$$

Proof: See the Appendix D.

The *Lemma* 3.1 provides a precondition to check that if $\varepsilon \leq \lambda_z / c_2 \chi_z$ is satisfied, then the discrepancy between the nominal boundary layer and the boundary layer dynamics exponentially decays to a bounded space (see Fig.7).

Similarly, replacing $y(t)$ with $z(t) - \vartheta(t)$, bounding $||y_n|| \leq y_0$ and using triangle inequality we can obtain the discrepancy between the trajectories $z(t)$ of the original full-order system and the slow manifold $\vartheta(t)$ as:

$$||z(t) - \vartheta(t)|| \leq \chi_z e^{(-\frac{\lambda_z - \varepsilon c_2 \chi_z}{\varepsilon})t}||z(0) - \vartheta(0)|| + \frac{(c_1 + c_2 y_o)\chi_z}{\lambda_z - \varepsilon c_2 \chi_z}\varepsilon + y_o. \tag{27}$$

Now, to obtain the expression on the discrepancy between the state of the full-order and the reduced-order model ($||x(t) - x_{red}(t)||$), the $x(t)$ dynamics in (19) may be rewritten as:

$$\dot{x} = f(x,\vartheta,t) + f(x,z,t) - f(x,\vartheta,t). \tag{28}$$

Using (25) in (28) and after simple manipulation, the following expression can be obtained as

$$||\dot{x}|| \leq ||f(x,\vartheta,t)|| + \alpha_1||z-\vartheta||. \tag{29}$$

It can be observed that the expression in (29) obtained from the full-order slow state variable dynamics ($\dot{x}$ from (19)) is a perturbed dynamics of the reduced-order expression (20). Thus, if the states of the reduced-order model (20) converge with the corresponding slow state variables of the full-order system, then the reduced-order model can be ~~said~~ to be valid. The following theorem provides the bounds on the discrepancy between the states of the reduced-order model and that of the full-order system.

Theorem 3.2: Let the premises of the *Lemma* 3.1 hold true for the SPS (19), and the reduced-order dynamics (20) is partially contracting in $x_{red}(t)$ with a transformation metric Θ_x. If the SPP satisfies the condition

$$\varepsilon \leq \frac{\lambda_z}{c_2 \chi_z}; \tag{30}$$

then the states of the reduced-order model exponentially converge towards the trajectories of the corresponding full-order system, and these bounds may be quantified as:

$$||x(t) - x_{red}(t)|| \leq \chi_x||x(0) - x_{red}(0)||e^{-\lambda_x t} + \varepsilon(C_{x2}(1 - e^{-\lambda_x t}) + C_{x1}(e^{-\lambda_x t} - e^{\frac{-(\lambda_z - \varepsilon c_2 \chi_z)}{\varepsilon}t})) \tag{31}$$

where $C_{x1} = \frac{\chi_x \alpha_1 \chi_z ||z(0) - \vartheta(x(0))||}{\lambda_z - \varepsilon c_2 \chi_z - \varepsilon \lambda_x}$, $C_{x2} = \frac{\chi_x \alpha_1}{\lambda_x}(\frac{(c_1 + c_2 y_o)\chi_z \varepsilon}{\lambda_z - \varepsilon c_2 \chi_z} + y_o)$.

Proof: With $Q(t) = ||\Theta_x(x(t) - x_{red}(t))||$ and using (29) and (20) we have $\dot{Q}(t) \leq F_x Q(t) + \alpha_1||z-\vartheta||$, where $F_x = (\dot{\Theta}_x + \Theta_x \frac{\partial f}{\partial x})\Theta_x{}^{-1}$. Further, using (27) and following the procedure similar to Appendix D, the expression (31) can be obtained.

From the discrepancy expression (31), the gain C_{x1} determines the steady state discrepancy bound, and other terms determine the transients.

The upper bound on the discrepancy between the states shown in (31) is found to be less conservative (see Table III) than that given in [19]–[22]. This can be explained by comparing the denominators of the terms C_{x1} and C_{x2}, which have $\lambda_z - c_2\varepsilon$ instead of only λ_z. This is achieved by relaxing the conservative bounds on $||\frac{\partial \vartheta}{\partial x} f(x,z,t)||$ in (24).

D. Convergence Analysis of SPS Under Modeling Uncertainties

Similarly, the parameters that are not associated with SPP may vary for different reasons. Let us capture these variations into modeling uncertainty terms and obtain certain validating conditions as in *Theorem* 3.2.

1) Uncertainties in z− subsystem: Let us consider a case in which the fast subsystem is perturbed by an additive uncertainty, i.e,

$$\varepsilon\dot{z} = g(x,z,\varepsilon) + \Delta g(x,z,\varepsilon). \tag{32}$$

The boundary layer dynamics in this case becomes

$$\varepsilon\dot{y} = g(x,y+\vartheta,\varepsilon) + \Delta g(x,y+\vartheta,\varepsilon) - \varepsilon\frac{\partial\vartheta}{\partial x}f(x,z,t) \tag{33}$$

where the modeling uncertainty term $\Delta g(x,z,\varepsilon)$ is a function of two states: $x(t)$ and $z(t)$. By comparing the (33) and (22), it can be observed that the perturbation to the nominal boundary layer dynamics is augmented by the term $\Delta g(x,z,\varepsilon)$.

The bounds on $\Delta g(x,z,\varepsilon)$ can be obtained similarly to the previous section by exploiting the timescale separation between $x(t)$ and $z(t)$. The bound can be obtained as $\Delta g(x,z,\varepsilon) \leq c_3||z|| + c_4$, and after simplification can also be expressed as $\Delta g(x,y+\vartheta,\varepsilon) \leq c_3||y|| + c_4'$, where $c_4' = c_4 + c_3||\vartheta||$. Thus, the bound on perturbation term to the nominal boundary layer dynamics in this case can be given as:

$$||\Delta g(x,y+\vartheta,\varepsilon) - \varepsilon\frac{\partial\vartheta}{\partial x}f(x,z,t)|| \leq \varepsilon(c_1' + c_2||y||) + c_3||y||. \tag{34}$$

where $c_1' = c_1 + \frac{c_4'}{\varepsilon}, c_2, c_3 \in R^+$.

Using *Lemma* 3.1, it can be derived that the trajectories of perturbed boundary layer dynamics (33) converge towards the trajectories of nominal dynamics (22), if the condition (35) is satisfied:

$$c_3\chi_z + \varepsilon c_2\chi_z \leq \lambda_z \Rightarrow \varepsilon \leq \frac{1}{c_2}(\frac{\lambda_z}{\chi_z} - c_3). \tag{35}$$

It can be observed that the uncertainty term $\Delta g(x,z,\varepsilon)$ modifies the previous bounding condition (30) by deducting it with $\frac{c_3}{c_2}$ (see Fig.8(a)), where c_3 is contributed by the upper bound of $\Delta g(x,z,\varepsilon)$.

Thus, the bounds on $||y(t) - y_n(t)||$, $||z(t) - \vartheta(x(t))||$ and $||x(t) - x_{red}(t)||$ can be obtained following a similar procedure as is carried out in the previous section. The robustness result for the validity of the reduced-order model under $\Delta g(x,z,\varepsilon)$ is given in the following theorem.

Theorem 3.3: Let the z-subsystem of the SPS (19) be associated with uncertainties as shown in (32). Assume that the uncertainty term is bounded as $\Delta g(x,y+\vartheta,\varepsilon) \leq c_3||y|| + c_4'$ and the reduced-order dynamics (20) is partially contracting in $x_{red}(t)$, with a transformation metric Θ_x and a contraction rate λ_x. If the SPP satisfies the condition (35), then the convergence of the state trajectories between the reduced-order model $x_{red}(t)$ (20) with that of the uncertain full-order system (19) occurs. Moreover, the discrepancies between the states may be quantified as (36):

$$\begin{aligned}||x(t) - x_{red}(t)|| \leq \chi_x||x(0) - x_{red}(0)||e^{-\lambda_x t} + \varepsilon(C_{x1}(e^{-\lambda_x t} \\ - e^{-(\frac{\lambda_z - \varepsilon c_2\chi_z - c_3\chi_x}{\varepsilon})t}) + C_{x2}(1 - e^{-\lambda_x t}))\end{aligned} \tag{36}$$

where $C_{x2} = \frac{\chi_x\alpha_1}{\lambda_x}\left(\frac{(c_1'+c_2y_0)\chi_z\varepsilon + c_3y_0\chi_z}{\lambda_z - c_3\chi_z - \varepsilon c_2\chi_z} + y_0\right)$ and $C_{x1} = \frac{\chi_x\alpha_1\chi_z||z(0)-\vartheta(x(0))||}{\lambda_z - \varepsilon c_2\chi_z - c_3\chi_z - \varepsilon\lambda_x}$.

Proof: Consider the nominal system (22) and the perturbed system (33). Following the proof in Appendix D, The perturbation term can be written as $d_\vartheta = \Delta(x,y+\vartheta,\varepsilon) - \varepsilon\frac{\partial\vartheta}{\partial x}f(x,z,t)$, whose upper bound is given as (34). The discrepancy $||z-\vartheta||$, can be derived following similar line of arguments as given in the Appendix D. Define $Q(t) \leq ||\Theta_x(x(t) - x_{red}(t))||$ and using (29) and (20), we have $\dot{Q}(t) = F_xQ(t) + \alpha_1||z-\vartheta||$. In this case, the expression (27) is slightly modified as in (33) and following the procedure similar to Appendix D the expression (36) is obtained.

Comparing the discrepancy expression (31) and (36), it can be observed that the modeling uncertainty in $z-$subsystem alters both the transient and steady-state bounds as the gains C_{x1}, C_{x2} and the exponential terms associated with the gain C_{x1} are changed.

2) Uncertainties in the x−subsystem: Further, let us now consider that the slow subsystem in (19) is associated with modeling uncertainties along with the fast subsystem and is represented as:

$$\dot{x} = f(x,z,t) + \Delta f(x,z,t). \tag{37}$$

The boundary layer dynamics (21) in this case where the modeling uncertainties are present in both the dynamics of $x(t)$ (37) and $z(t)$ (32) is given as:

$$\begin{aligned}\varepsilon\dot{y} = g(x,y+\vartheta,\varepsilon) + \Delta g(x,y+\vartheta,\varepsilon) \\ - \varepsilon\frac{\partial\vartheta}{\partial x}(f(x,z,t) + \Delta f(x,z,t))\end{aligned} \tag{38}$$

It can be observed that the perturbation to the nominal boundary dynamics (22) in this case is given by the term $\Delta g(x,y+\vartheta,\varepsilon) - \varepsilon\frac{\partial\vartheta}{\partial x}(f(x,z,t) + \Delta f(x,z,t))$.

Exploiting the timescale difference, the term $\Delta f(x,z,t)$ can be bounded in terms of the state $x(t)$ as $\|\Delta f(x,z,t)\| \leq d_1 + d_2\|x\|$, where $d_1, d_2 \in R^+$, and

$$||\frac{\partial\vartheta}{\partial x}\Delta f(x,y+\vartheta,t)|| \leq d_2c_{d1}||y|| + c_{d2} \tag{39}$$

where $c_{d2} = (d_1 + d_2c_d||\vartheta||)||\frac{\partial\vartheta}{\partial x}||$, $c_{d1} = c_d||\frac{\partial\vartheta}{\partial x}||$. Using (34) and (39), the bound on the perturbation term in the expression (38) is given as:

$$\begin{aligned}||\Delta g(x,y+\vartheta,\varepsilon) - \varepsilon\frac{\partial\vartheta}{\partial x}(f(x,z,t) + \Delta f(x,y+\vartheta,t))|| \\ \leq \varepsilon((c_1' + c_{d2}) + (c_2 + d_2c_{d1})||y||) + c_3||y||\end{aligned} \tag{40}$$

Exploiting the *Lemma* 3.1 and proceeding along similar lines, it can be derived that the trajectory of the perturbed boundary layer dynamics (38) converges with that of the nominal one (22) when the condition (44) is satisfied

$$\varepsilon \leq \frac{1}{(c_2 + d_2c_{d1})}(\frac{\lambda_z}{\chi_z} - c_3). \tag{41}$$

The modeling uncertainty $\Delta f(x,z,t)$ further modifies the bounding condition on SPP. When compared with the condition (35), the bounding on SPP is decreased further with an increase in the denominator part of the expression (41).

However, in contrast to the previous sections, the expression in (28) is now associated with additional terms as shown in (42):

$$\dot{x} = f(x,\vartheta,t) + f(x,z,t) - f(x,\vartheta,t) + \Delta f(x,z,t). \tag{42}$$

As the state $x(t)$ can be bounded through the triangle inequality as $\|x\| \leq \|x - x_{red}\| + \|x_{red}\|$, the bounds on $\Delta f(x,z,t)$ can be given as:

$$\Delta f(x,z,t) \leq d_1^{'} + d_2||x - x_{red}||. \tag{43}$$

where $d_1' = d_1 + ||x_{red}||d_2$.

The result for the convergence of the reduced-order model with its full-order system under uncertainties in the $x-$subsystem is given by the following theorem.

Theorem 3.4: For an uncertain SPS (19), whose z and x subsystems are represented as (32) and (37) respectively, let the hypothesis of the *Theorem* 3.3 holds true. If the SPP satisfy the condition (41) and d_2 in (43) satisfies

$$d_2 \leq \frac{\lambda_x}{\chi_x}, \tag{44}$$

then the validity of the reduced-order model (15) holds true. Further, the discrepancies can be quantified as:

$$\begin{aligned}\|x(t) - x_{red}(t)\| \leq \chi_x \|x(0) - x_{red}(0)\| e^{-(\lambda_x - d_2\chi_x)t} \\ + \varepsilon C_{x2}(1 - e^{-(\lambda_x - d_2\chi_x)t}) \\ + \varepsilon C_{x1}(e^{-(\lambda_x - d_2\chi_x)t} - e^{-(\frac{\lambda_z - \chi_z(\varepsilon(c_2+c_{d1})+c_3)}{\varepsilon})t})\end{aligned} \tag{45}$$

where $C_{x1} = \frac{\chi_x\alpha_1\chi_z\|z(0)-\vartheta_x(0)\|}{\lambda_z-(\varepsilon(c_2+d_2c_{d1})+c_3)\chi_z-\varepsilon(\lambda_x-d_2\chi_x)}$, $C_{x2} = \left(\frac{((c_1'+c_{d2})+(c_2+d_2c_{d1})y_0)\varepsilon+c_3y_0\chi_z}{\lambda_z-c_3\chi_z-\varepsilon(c_2+d_2c_{d1})\chi_z} + y_0 + d_1'\right)\frac{\alpha_1}{\lambda_x-d_2\chi_x}$.

Proof: Using (42) and (43), the inequality is obtained as $||\dot{x}|| \leq ||f(x,\vartheta,t)|| + \alpha||z-\vartheta|| + d_1^{'} + d_2||x - x_{red}||$. Using this inequality appropriately as in the proof of *Lemma*3.1 and considering $Q(t) = ||\Theta_x(x(t) - x_{red}(t))||$ we have $||\dot{Q}(t)|| \leq F_xQ(t) + d_2Q(t) + \alpha(||z-\vartheta|| + d_1^{'})$. Further, solving using the matrix measure on F_x, the discrepancy expression can be obtained as (45).

It should be noted that when the $x-$subsystem is associated with modeling uncertainties then, in addition to the bounding condition on the SPP (41), there is an additional bounding condition on the uncertainty term $\Delta f(x,z,t)$ given by (44). However, the trajectory of the uncertain SPS (32) and (37) still converge towards the reduced order system (20).

E. A Linear System Case

A linear time-invariant (L.T.I.) system with modeling uncertainties as $\Delta_1(x,z)$ and $\Delta_2(x,z)$ is represented in (46):

$$\begin{aligned}\dot{x} &= A_{11}x + A_{12}z + \Delta_1(x,z) \\ \varepsilon\dot{z} &= A_{21}x + A_{22}z + \Delta_2(x,z)\end{aligned} \tag{46}$$

The obtained results in *Theorem* 3.2, *Theorem* 3.3 and *Theorem* 3.4 can be extended for the linear system (46). The reduced-order system for (46) is given as (47):

$$\dot{x}_{red} = A_{red}x_{red} \tag{47}$$

where $A_{red} = A_{11} - A_{12}{A_{22}}^{-1}A_{21}$.

The slow manifold for the system (46) is given as $\vartheta = -A_{22}^{-1}A_{21}x$, the Lipschitz constant (α_1) is bounded as $\alpha_1 \geq ||A_{12}||$ and the nominal boundary layer dynamics is given as $\dot{y}_n = A_{22}y_n$.

For an L.T.I. system (46), the associated transformation matrix Θ can be considered as $\Theta = I$ [26]. Then, the resulting contraction condition can be given as $A + A^T \leq \beta I$. Using the Rayleigh inequality, we can assign $\beta = 2(max\{\lambda\})$, where λ is the maximum value of the eigenvalue of A. Thus, the $\lambda_z = 2(max\ eigenvalue\ of\ A_{22})$ and $\lambda_x = 2(max\ eigenvalue\ of\ A_{11})$ for the (46). For the system (46) without uncertainties i.e Δ_1 =0 and Δ_2 =0, the bounds on the boundary layer dynamics is obtained as:

$$\varepsilon\dot{y} \leq A_{22}y + \varepsilon(c_1 + c_2y) \tag{48}$$

where $c_2 = ||{A_{22}}^{-1}A_{21}A_{12}||$ and $c_1 = ||{A_{22}}^{-1}A_{21}(A_{11} - A_{12}A_{22}^{-1}A_{21})||||x||$.

If Δ_1 and Δ_2 terms are included, then appropriate changes may be easily incorporated through the addition of bounding terms $\Delta_2(x,z) \leq c_4 + c_3||z||$ and $\Delta_1(x,z) \leq d_1 + d_2||x||$. Under such a case, the c_d, c_{d1} and c_{d2} in the expressions (39) may be defined as $c_d = ||(A_{21}^TA_{21})^{-1}A_{21}^TA_{22}||$, $c_{d1} = ||(A_{21}^TA_{21})^{-1}A_{21}^TA_{22}||||A_{22}^{-1}A_{21}||$ and $c_{d2} = d_1 + d_2c_d||A_{22}^{-1}A_{21}||^2||x||$.

IV. Convergence Analysis in the IBMG System

After obtaining the theoretical results in the form of *Theorem* 3.2, *Theorem* 3.3 and *Theorem* 3.4 on the discrepancy between a reduced-order model with its uncertain full-order system, in this section these are used to analyze the reduced-order model (15) validity with respect to the uncertain full-order IBMG system (1).

A. Uncertain Cases in IBMG

1) Case 1: Uncertainty in SPP Parameters: The parameters that are defining ε_1 and ε_2 are shown in Table I. The effect of uncertainties in these parameters on the validity of the reduced-order model is studied using the results obtained in *Theorem* 3.2.

It should be noted that for any variations in the system parameters the contraction rate λ_z and c_2 in the condition (30) will change. Table II summarizes the parameter uncertainties bounds under which the condition (30) is satisfied. The convergence and divergence trajectories of discrepancies with respect to the condition (30) are plotted in Fig.7. It can be observed from Fig.7 that for any uncertainties in the parameters governing SPP, the convergence between the state trajectories of the reduced-order model and full-order system holds true until the condition (30) is satisfied. These results presented in Table II would not have been possible with the approach followed in [19]–[22].

Table II shows the bounds on IBMG parameter uncertainties within which the convergence occurs but does not say anything about the effect of parameter uncertainty on discrepancies. In many practical applications, it is desired that the discrepancy between the reduced-order model and the full-order model must be within a certain bound. In such cases, the expression given in (31) can be used to quantify the IBMG parameters' uncertainty bound.

TABLE II
UPPER BOUNDS OF PARAMETER UNCERTAINTY BEYOND WHICH (30) FAILS TO HOLD

Parameters (Nominal P_0)	Multiplicative Uncertainty ($\times\Delta P_0$)	ε_2	λ_z	c_2
L_c	1.26×10^3	0.441×10^{-3}	0.547	1.24×10^3
L_{line1}	7×10^3	1.114×10^{-3}	0.258	0.232×10^3
Parameters (Nominal P_0)	Multiplicative Uncertainty ($\times\Delta P_0$)	ε_1	λ_z	c_2
C_f	3.3×10^2	1.65×10^{-2}	6.068	0.368×10^3
L_f	2.41	26×10^{-4}	747.4	3.619×10^5
K_{pc}	1/11	0.31×10^{-2}	330.84	2.4335×10^5
K_{iv}	1/4.9	1.62×10^{-2}	752.3	4.644×10^4

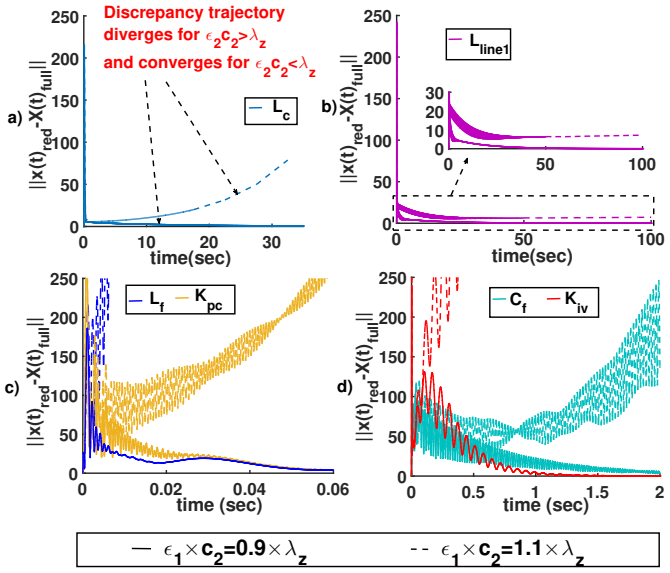

Fig. 7. The plot of discrepancy showing that when the given condition (30) is satisfied, then convergence occurs a) for ε_1 with uncertainty in L_c b) for ε_1 with uncertainty in L_{line1} c) for ε_2 with uncertainty in L_f and K_{pc} d) for ε_2 with uncertainty in C_f and K_{iv}.

To illustrate the above case, let the desired bound on the discrepancy due to uncertainties be given as 10%. In mathematical terms, this can be expressed as:

$$\frac{||x_{red}(t) - X_{fulluncertn}(t)||}{||x_{red}(t) - X_{fullnom}(t)||} \leq 110\% \tag{49}$$

where $x_{red}(t)$, $X_{fulluncertn}(t)$ and $X_{fullnom}(t)$ represent the obtained reduced-order model, full-order system with parameter uncertainties and full-order with nominal parameter, respectively.

Table III logs the IBMG parameters' uncertainty bound for a discrepancy less than 10% by using the iterative simulations method, the given expression (31) and the expression in [19]. From the listed bounds on the IBMG parameters in Table III, it can be observed that the bounds obtained using the expression (31) are much closer to those in the simulation than the bounds obtained through [19]. Thus, the expression (31) provides an updated and improved discrepancy expression compared with the one given in [19] and can be used to obtain

TABLE III
UPPER BOUND OF PARAMETER UNCERTAINTY SUCH THAT THE DISCREPANCY IS LESS THAN 10%

Parameters (Nominal P_0)	Simulation	Using (31)	Using [19]
	$+\Delta P_0$ (Additive Uncertainty)		
L_c	8.15×10^{-6}	7.58×10^{-6}	6.32×10^{-6}
L_{line1}	0.0997	0.0926	0.0782
L_{line2}	1×10^{-4}	0.926×10^{-4}	0.816×10^{-4}
C_f	1.745×10^{-5}	1.702×10^{-5}	1.340×10^{-5}
L_f	9.5×10^{-4}	9.2×10^{-4}	6.17×10^{-4}
K_{pc}	-9.52	-9.31	-7.54
K_{iv}	-17.55	-17.23	-14.15

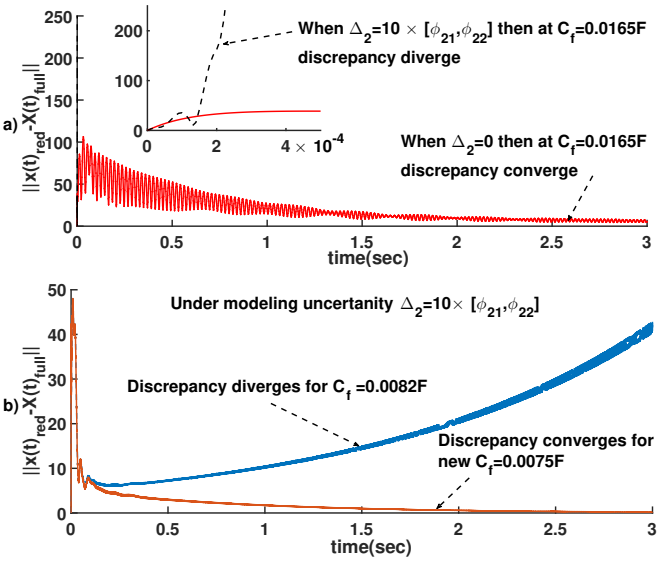

Fig. 8. Discrepancy behavior for modeling uncertainty in z-dynamics (Δ_2) a) The bounds on the parameter C_f decrease with uncertainty $\Delta_2 = 10\times[\phi_{21}\,\phi_{22}]$ b) The new bound on parameter C_f is 0.0076F.

the parameter uncertainty bound such that the discrepancy is within the desired limit.

2) Case 2: Robustness to Modeling Uncertainty: Let the parametric uncertainties that are not associated with SPP (ε) be represented through modeling uncertainties Δ_1 and Δ_2 as shown in the expression (46). Assuming that the unmodeled dynamics associated with the IBMG (4) are Lipschitz in nature and satisfy the condition similar to (24) (discussed in Section III-D), the validity of the reduced-order model (15) can be realized through the results given in *Theorem* 3.3 and *Theorem* 3.4.

a) Modeling Uncertainties in $z-$dynamics: The condition (35) on SPP shows that the modeling uncertainty in $z-$dynamics decreases the SPP bound given in (30) by a factor of $\frac{c_3}{c_2}$. This implies that the bounds on IBMG parameter uncertainties presented in Table II will decrease for the modeling uncertainty present in $z-$dynamics. This effect can be demonstrated in Fig.8(a) for the parameter C_f of the IBMG under the modeling uncertainty $\Delta_2 = 10\times[\phi_{21}\ \phi_{22}\ 0]$. It can be observed that under the modeling uncertainty (Δ_2) the discrepancy trajectory diverges for the earlier obtained bound on the parameter C_f i.e $0.0165F$. The new bound for

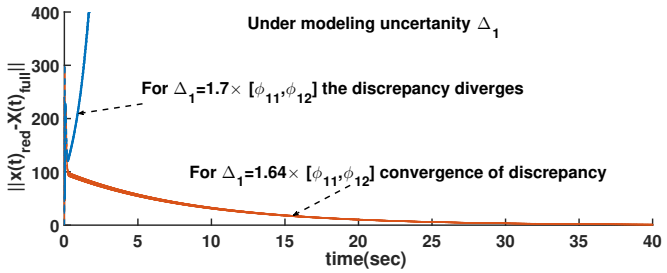

Fig. 9. Discrepancy behavior for modeling uncertainty in x-dynamics (Δ_1).

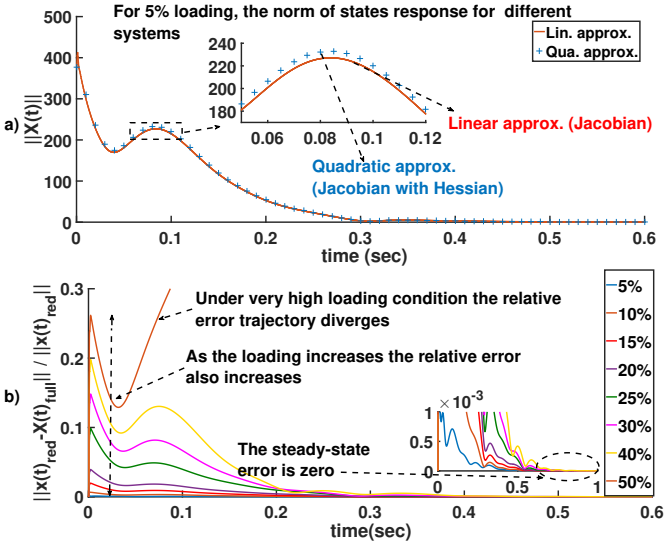

Fig. 10. The effect of high loading condition a) Plot of states norm trajectories for linear and quadratic approximated models. b) Plot of relative discrepancy between the reduced-order model and full-order IBMG system for different loading conditions.

C_f under modeling uncertainty Δ_2 can be obtained using the expression (35), where $c_3 = 3.308$. The plot for discrepancy with $C_f = 0.0075F$ and $C_f = 0.0082F$ is shown in Fig.8(b). A similar analysis can be carried for other variables in Table II under certain modeling uncertainty Δ_2.

b) Modeling Uncertainty in x−dynamics: It has been shown in Section III-D that under the modeling uncertainty in $x-$ dynamics, the state trajectories of the reduced-order model and uncertain full-order system converge if the condition $d_2 \leq \lambda_x/\chi_x$ is satisfied. Let the microgrid dynamics (4) be associated with uncertainty $\Delta_1 = K_{factor}[\phi_{11}\ \ \phi_{12}\ \ 0]$, where K_{factor} determines the amount of uncertainty. The $d_2 = ||\phi_{11}|| = 38.3049$, $\lambda_x = 2 \times 31.41$, thus the $K_{factor} = 1.64$. The discrepancy trajectory plotted in Fig.9 shows that if the modeling uncertainty Δ_1 satisfies $d_2 \leq \lambda_x/\chi_x$ then convergence between the reduced-order system and the uncertain IBMG system occurs.

B. High Loading Condition

In all the above case studies 5%, perturbation from the operating condition, which is a light loading condition, is considered. In this case study, the effect of a high loading condition is examined.

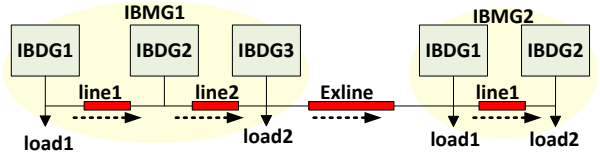

Fig. 11. Schematic diagram of the test MMGs.

Equation (1) is a linear model of an IBMG system. A large loading condition may shift the operating point, and its impact can be better analyzed by considering the nonlinear model. Let the nonlinear dynamics of the IBMG system be represented as:

$$\dot{X}_{MG} = f_{MG}(X_{MG}) \tag{50}$$

where the f_{MG} is the nonlinear function of the IBMG's states. Let us define the operating point of (50) as $X_{MG}(0)$. The Taylor series expansion of (50) around the operating point $X_{MG}(0)$ can be given as:

$$\dot{X}_{MG} = f_{MG}(X_{MG}(0)) + J(f_{MG})(X_{MG} - X_{MG}(0)) + 0.5I \otimes (X_{MG} - X_{MG}(0))^T H(f_{MG})(X_{MG} - X_{MG}(0)) + H.O.T., \tag{51}$$

where $J(f_{MG})$ and $H(f_{MG}) = \nabla J(f_{MG})$ are the Jacobian and Hessian matrix obtained on f_{MG}, respectively. The I is an identity matrix, and the operator ∇ and $\otimes$ are Gradient and Kronecker products, respectively, and $H.O.T.$ represents the higher-order terms. In the expression (51), the perturbation from the operating point is given by $X_{MG} - X_{MG}(0)$. It can be observed that the Taylor series expansion is dependent on perturbation and depending upon the amount of perturbation, an appropriate approximate model can be realized.

The norm of state response for 5% perturbation in the linear approximation model (neglecting the $H(f_{MG})$ and $H.O.T.$ as obtained in (1)) and quadratic approximation model (neglecting the $H.O.T.$) are plotted in Fig.10(a). It can be observed that both the trajectories are almost the same, thus for the 5% perturbation the nonlinear IBMG system may be approximated to a linear model to arrive at a simplistic expression. However, as the loading increases, the effect of the higher-order term becomes evident. Now, the reduced-order model (15) is obtained using the linear model (1) of IBMG. Thus, it is evident that, under high loading conditions, the error between the reduced-order model and the nonlinear IBMG system will increase with an increase in loading conditions. Fig.10(b) shows the relative error between the states of the reduced-order model and nonlinear IBMG system. It can be observed that the transient discrepancy increases under a high loading condition; however, the steady-state discrepancy reaches zero.

C. Reduced Order IBMG Model in MMGs Scenario

In all the above case studies, the discrepancy behavior between the reduced-order IBMG model and its full-order system has been analyzed for an autonomous system. In this

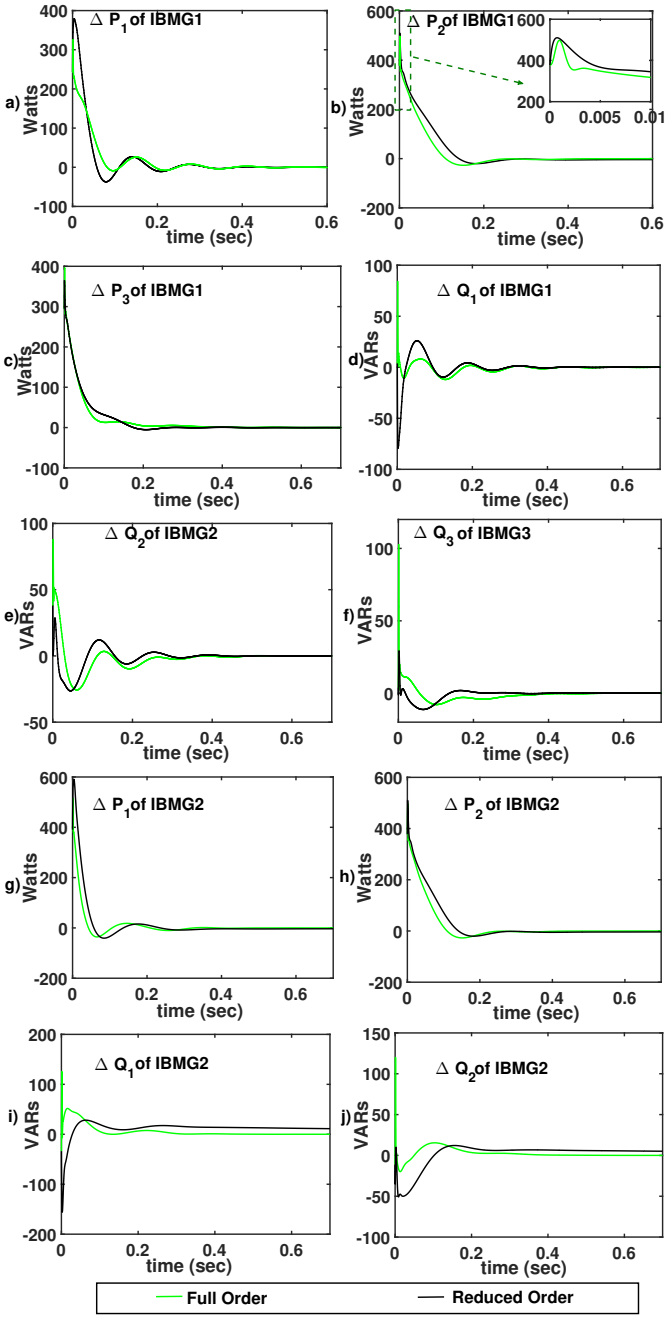

Fig. 12. Real and reactive power states trajectories for the full-order and the corresponding reduced-order MMG system a) ΔP_1 for IBMG1, b) ΔP_2 for IBMG1, c) ΔP_3 for IBMG1 d) ΔQ_1 for IBMG1 e) ΔQ_2 for IBMG1 f) ΔQ_3 for IBMG1 g) ΔP_1 for IBMG2 h) ΔP_2 for IBMG2 i) ΔQ_1 for IBMG2 j) ΔQ_2 for IBMG2.

case study, the behavior of the obtained reduced-order models for different IBMGs in an MMG scenario is examined. To examine this effect, a testbed of an MMG system is formulated as shown in Fig.11. The formulated MMGs consists of two IBMGs (IBMG1 and IBMG2) interconnected through an external network. IBMG1 is the same as that considered in Section II, and IBMG2 consists of two IBDGs. All the IBDGs have the same values for parameters, whereas the values for internal and external network parameters are given in the Table of Appendix C .

As the IBMGs are reduced in terms of the power control loop, the trajectories of the real and reactive power states for full- and reduced-order models are shown in Fig.12. It can be observed from Fig.12 that the states of the reduced-order IBMGs converge with their full-order counterparts within 0.2 seconds. However, if the states trajectories in Fig.12 are compared with Fig.3, it can be observed that the discrepancy during transient is higher in the MMG scenario than that of the autonomous IBMG. This result is expected because in the MMG scenario, the exogenous inputs to each IBMG (coupling effect between IBMGs) act like a disturbance.

V. Conclusion

This paper presents a quantitative analysis of the convergence behavior of a reduced-order IBMG model obtained through the SP method with its uncertain full-order system. To perform the quantitative analysis, new results in the form of theorems on discrepancy expressions for a generalized uncertain system have been developed by exploiting partial contraction theory. It is observed that the IBMG system exhibits multi-timescales behavior and can be reduced in terms of the power control loop using the SP method. The obtained reduced-order model is based on nominal system parameters of the IBMG, and its behavior can drastically differ from the full-order IBMG system associated with uncertainties in parameters. The discrepancy behavior and quantitative bounds on IBMG system parameters are achieved through the results in theorems. It is observed that for any uncertainty in parameters within the given bounds on SPP (30) the reduced-order model converges to the uncertain full-order IBMG system. Further, the effects of different loading conditions on the reduced-order model behavior with respect to its full-order counterpart are also analyzed. Finally, the efficacy of integrating different reduced-order IBMGs is examined in an MMG scenario. The extension of the proposed technique to deal with controller design aspects could be a subject for future studies.

Appendix A
Elements of the IBMG State Matrix

The elements of A_{mg} in (1) $\forall k \in \{1,2,3\}$ $\forall i \in \{1,2\}$ are:

$$A_{I_k} = \begin{bmatrix} a_{PP} & a_{PC} & a_{PV_0} & a_{Pi_0} \\ a_{CP} & a_{CC} & a_{CV_0} & a_{Ci_0} \\ a_{V_0P} & a_{V_0C} & a_{V_0V_0} & a_{V_0i_0} \\ a_{i_0P} & a_{i_0C} & a_{i_0V_0} & a_{i_0i_0} \end{bmatrix};$$

$$a_{PP} = \begin{bmatrix} 0 & -m_p & 0 \\ 0 & -\omega_c & 0 \\ 0 & 0 & -\omega_c \end{bmatrix}; a_{PC} = [0]_{(3\times 6)};$$

$$a_{PV_o} = \begin{bmatrix} 0 & 0 \\ \omega_c I_{od_k} & \omega_c I_{oq_k} \\ -\omega_c I_{oq_k} & \omega_c I_{od_k} \end{bmatrix} \quad a_{Pi_o} = \begin{bmatrix} 0 & 0 \\ \omega_c V_{od_k} & \omega_c V_{oq_k} \\ \omega_c V_{oq_k} & -\omega_c V_{od_k} \end{bmatrix};$$

$$a_{CP} = \begin{bmatrix} 0 & 0 & -n_q \\ 0 & 0 & 0 \\ 0 & 0 & -n_q K_{pc} \\ 0 & 0 & 0 \\ 0 & -m_p I_{lq} & 0 \\ 0 & m_p I_{ld} & 0 \end{bmatrix};$$

$$a_{CC} = \begin{bmatrix} [0]_{2\times2} & [0]_{2\times2} & [0]_{2\times2} \\ K_{iv}[I]_{2\times2} & [0]_{2\times2} & -[I]_{2\times2} \\ \frac{K_{pc}K_{iv}}{L_f}[I]_{2\times2} & \frac{K_{ic}}{L_f}[I]_{2\times2} & \begin{bmatrix} a_{CC(5,5)} & a_{CC(5,6)} \\ a_{CC(6,5)} & a_{CC(6,6)} \end{bmatrix} \end{bmatrix};$$

where $a_{CC(5,5)} = a_{CC(6,6)} = \frac{-r_f - K^2{}_{pc}}{L_f}$, $a_{CC(6,5)} = -\omega_0 + \omega_n K_{pc}$ and $a_{CC(6,6)} = \omega_0 - \omega_n K_{pc}$.

$$a_{CV_0} = \begin{bmatrix} -1 & 0 \\ 0 & -1 \\ -K_{PV} & -\omega_n C_f \\ \omega_n C_f & -K_{PV} \\ \frac{-1-K_{pc}K_{pv}}{L_f} & \frac{-\omega_n C_f K_{pc}}{L_f} \\ \frac{\omega_n C_f K_{pc}}{L_f} & \frac{-1-K_{pc}K_{pv}}{L_f} \end{bmatrix}; a_{Ci_0} = \begin{bmatrix} [0]_{(2\times2)} \\ F[I]_{(2\times2)} \\ \frac{FK_{pc}}{L_f}[I]_{(2\times2)} \end{bmatrix};$$

$$a_{V_0P} = \begin{bmatrix} 0 & -m_p V_{oq_k} & 0 \\ 0 & m_p V_{od_k} & 0 \end{bmatrix} \quad a_{V_0C} = \begin{bmatrix} [0]_{(4\times2)} \\ (1/c_f)[I] \end{bmatrix}^T;$$

$$a_{V_0V_0} = \begin{bmatrix} 0 & \omega_0 \\ -\omega_0 & 0 \end{bmatrix}; a_{V_0i_0} = (-1/c_f)[I]_{(2\times2)};$$

$$a_{i_0P} = \begin{bmatrix} \frac{-V_{bD_k}sin\delta_k + V_{bQ_k}cos\delta_k - I_{oq_k}r_n}{L_c} & -m_p I_{oq_k} & 0 \\ \frac{-V_{bD_k}cos\delta_k - V_{bQ_k}sin\delta_k - I_{od_k}r_n}{L_c} & m_p I_{od_k} & 0 \end{bmatrix};$$

$$a_{i_0C} = [0]_{(2\times6)}; a_{i_0V_0} = 1/L_c[I]_{(2\times2)};$$

$$a_{i_0i_0} = \begin{bmatrix} \frac{-r_{LC}+r_n}{L_c} & \omega_0 \\ -\omega_0 & \frac{-r_{LC}+r_n}{L_c} \end{bmatrix};$$

$$A_{L_i} = \begin{bmatrix} \frac{-r_{line_i}-2r_n}{L_{line_i}} & \omega_0 \\ -\omega_0 & \frac{-r_{line_i}-2r_n}{L_{line_i}} \end{bmatrix};$$

$$B_{I_iI_1} = \begin{bmatrix} 0 & m_p & [0] \\ [0 & 0 & 0]_{(12\times13)} \end{bmatrix}; B_{L_iL_{3-i}} = \frac{r_n}{L_{line_i}}[I]_{(2\times2)};$$

$$B_{L_iI_{1_0}} = \begin{bmatrix} 0 & -m_p I_{lineQ_i} & \begin{bmatrix} 0 \\ 0 \end{bmatrix}_{4\times11} \\ 0 & m_p I_{lineD_i} & \end{bmatrix};$$

$$B_{I_kL_i} = (-1)^{k+i+1}\frac{r_n}{L_c}\begin{bmatrix} [0 & 0]_{(11\times2)} \\ cos\delta_k & sin\delta_k \\ -sin\delta_k & cos\delta_k \end{bmatrix};$$

$$B_{L_iI_k} = K\begin{bmatrix} (-I_{od_k}sin\delta_k - I_{oq_k}cos\delta_k) & [0]_{(1\times10)} & [cos\delta_k & -sin\delta_k] \\ (I_{od_k}cos\delta_k - I_{oq_k}cos\delta_k) & [0]_{(1\times10)} & [sin\delta_k & cos\delta_k] \end{bmatrix};$$

where $K = (-1)^{(i+k)}\frac{r_n}{L_{line_i}}$.

Appendix B
Elements of MMGs Dynamics (18)

$$A_{MG_ired} = \varphi_{MG_i(1,1)} - \varphi_{MG_i(1,2)}\varphi^{-1}_{MG_i(2,2)}\varphi_{MG_i(2,1)} \quad (52)$$

$$B_{MG_iExNred} = \varphi_{MG_i(1,2)}\varphi^{-1}_{MG_i(2,2)}\psi_{MG_iExN(2)} \quad (53)$$

$$A_{ExNred} = \sum_{i=1}^{n}\psi_{ExNMG_i(2)}\varphi^{-1}_{MG_i(2,2)}\psi_{MG_iExN(2)} - \varphi_{ExN} \quad (54)$$

$$B_{ExNMG_ired} = \sum_{i=1}^{n}\psi_{ExNMG_i(1)} - \sum_{i=1}^{n}\psi_{ExNMG_i(2)}\varphi^{-1}_{MG_i(2,2)}\varphi_{MG_{i(2,1)}} \quad (55)$$

$$B_{MG_ired\omega_{com}} = \psi_{MG_i\omega_{com}(1)} - \varphi_{MG_i(1,2)}\varphi^{-1}_{MG_i(2,2)}\psi_{MG_i\omega_{com}(2)} \quad (56)$$

Appendix C
Nominal Values of IBMG Parameters

TABLE IV
Inverter Parameters Nominal Value (P_0)

m_p	9.4e-5	K_{iv}	390	ω_c	31.41
n_q	1.3e-3	K_{ic}	16000	F	0.75
K_{pv}	0.05	C_f	50e-6 F	L_c	0.35e-3 H
K_{pc}	10.5	r_f	0.1 ohm	L_f	1.35e-3 H
ω_0	2π50 rad/sec				

TABLE V
Network Parameters

Internal	IBMG#1		
X_{Line1}	0.1 ohm	R_{Line1}	0.23 ohm
X_{Line2}	0.58 ohm	R_{Line2}	0.35 ohm
Internal	IBMG#2		
X_{Line3}	0.58 ohm	R_{Line3}	0.35 ohm
External			
$X_{ExLine1}$	0.3 ohm	$R_{ExLine1}$	0.69 ohm

TABLE VI
Load Parameters

IBMG#1	ohm		H	IBMG#2	ohm		H
R_{Load1}	25	L_{Load1}	0	R_{Load1}	15	L_{Load1}	0
R_{Load2}	20	L_{Load2}	0	R_{Load2}	20	L_{Load2}	0

Appendix D
Proof of *Lemma* 3.1:

The nominal contracting dynamics is $\varepsilon\dot{y}_n = g(x, y_n + \vartheta, \varepsilon)$, and the perturbed contracting dynamics is expressed as $\varepsilon\dot{y} = g(x, y+\vartheta, \varepsilon) + \varepsilon d_\vartheta$, where $d_\vartheta = -\frac{\partial\vartheta}{\partial x}f(x,z,t)$. Hence, we can write:

$$\varepsilon\frac{d}{dt}(y - y_n) = g(x, y+\vartheta, \varepsilon) - g(x, y_n+\vartheta, \varepsilon) + \varepsilon d_\vartheta. \quad (57)$$

By defining a variation $\int \delta y = y - y_n$, the differential dynamics of (57) can be derived as [26], [28]:

$$\varepsilon\delta\dot{y} = \frac{\partial g}{\partial y}\delta y + \varepsilon d_\vartheta. \quad (58)$$

As the nominal system is contracting with a transformation metric Θ_z, a new variation can be defined as

$$\delta\omega = \Theta_z\delta y \quad (59)$$

whose derivative can be derived as:

$$\varepsilon\delta\dot{\omega} = \underbrace{(\varepsilon\dot{\Theta}_z + \Theta_z\frac{\partial g}{\partial y})\Theta_z{}^{-1}}_{F_z}\delta\omega + \varepsilon\Theta_z d_\vartheta. \quad (60)$$

Taking the norm on both sides and by the negative definiteness of F_z ($F_z + F_z^T \leq -\lambda_z I$, where $\lambda_z \in R^+$),

$$\varepsilon||\delta\dot{\omega}|| \leq -\lambda_z||\delta\omega|| + \varepsilon||\Theta_z d_\vartheta||. \tag{61}$$

Let $r_1 = \int||\delta y||$ and $r_2 = \int||\delta\omega||$. From the definition (59),

$$||\Theta_z||^{-1} r_2 \leq r_1 \leq ||\Theta_z^{-1}||r_2, \tag{62}$$

and the finite gain property of d_ϑ (24),

$$||d_\vartheta|| \leq c_1 + c_2||y|| \leq c_1 + c_2||y - y_n|| + c_2 y_o, \tag{63}$$

where y_o is the forward bounded solution of y_n. Therefore, the following can be derived using (61), (62) and (63)

$$\varepsilon\dot{r}_2 \leq -\lambda_z r_2 + \varepsilon||\Theta_z||(c_2 r_1 + c_1 + c_2 y_o), \tag{64}$$

$$\varepsilon\dot{r}_2 \leq -\lambda_z r_2 + \varepsilon||\Theta_z||(c_2||\Theta_z^{-1}||r_2 + c_1 + c_2 y_o)), \tag{65}$$

$$\varepsilon\dot{r}_2 \leq -\lambda_z r_2 + \varepsilon\chi_z c_2 r_2 + \varepsilon||\Theta_z||(c_1 + c_2 y_o). \tag{66}$$

where χ_z is the condition number of Θ_z. Using $\delta y = {\Theta_z}^{-1}\delta\omega$ and (62) in (66), further integrating over time the bound (26) can be obtained.

References

[1] R. H. Lasseter, "Smart distribution: Coupled microgrids," *Proceedings of the IEEE*, vol. 99, no. 6, pp. 1074–1082, June 2011.

[2] Z. Shuai, Y. Peng, X. Liu, Z. Li, J. M. Guerrero, and Z. J. Shen, "Dynamic equivalent modeling for multi-microgrid based on structure preservation method," *IEEE Transactions on Smart Grid*, vol. 10, no. 4, pp. 3929–3942, July 2019.

[3] Y. Wang, P. Liu, D. Liu, F. Deng, and Z. Chen, "Enhanced hierarchical control framework of microgrids with efficiency improvement and thermal management," *IEEE Transactions on Energy Conversion*, pp. 1–1, 2020.

[4] M. S. Golsorkhi, Q. Shafiee, D. D. Lu, and J. M. Guerrero, "Distributed control of low-voltage resistive ac microgrids," *IEEE Transactions on Energy Conversion*, vol. 34, no. 2, pp. 573–584, 2019.

[5] R. Wang, Q. Sun, P. Zhang, Y. Gui, D. Qin, and P. Wang, "Reduced-order transfer function model of the droop-controlled inverter via jordan continued-fraction expansion," *IEEE Transactions on Energy Conversion*, pp. 1–1, 2020.

[6] V. Purba, B. B. Johnson, M. Rodriguez, S. Jafarpour, F. Bullo, and S. V. Dhople, "Reduced-order aggregate model for parallel-connected single-phase inverters," *IEEE Transactions on Energy Conversion*, vol. 34, no. 2, pp. 824–837, 2019.

[7] L. Luo and S. V. Dhople, "Spatiotemporal model reduction of inverter-based islanded microgrids," *IEEE Transactions on Energy Conversion*, vol. 29, no. 4, pp. 823–832, Dec 2014.

[8] I. P. Nikolakakos, H. H. Zeineldin, M. S. El-Moursi, and N. D. Hatziargyriou, "Stability evaluation of interconnected multi-inverter microgrids through critical clusters," *IEEE Transactions on Power Systems*, vol. 31, no. 4, pp. 3060–3072, July,2016.

[9] V. Mariani, F. Vasca, J. C. Vásquez, and J. M. Guerrero, "Model order reductions for stability analysis of islanded microgrids with droop control," *IEEE Transactions on Industrial Electronics*, vol. 62, no. 7, pp. 4344–4354, July 2015.

[10] M. Rasheduzzaman, J. A. Mueller, and J. W. Kimball, "Reduced-order small-signal model of microgrid systems," *IEEE Transactions on Sustainable Energy*, vol. 6, no. 4, pp. 1292–1305, Oct. 2015.

[11] S. Gugercin and A. Antoulas, "A comparative study of 7 algorithms for model reduction," in *Proceedings of the 39th IEEE Conference on Decision and Control (Cat. No. 00CH37187)*, vol. 3. IEEE, 2000, pp. 2367–2372.

[12] T. Ersal, H. K. Fathy, D. G. Rideout, L. S. Louca, and J. L. Stein, "A review of proper modeling techniques," *Journal of Dynamic Systems, Measurement, and Control*, vol. 130, no. 6, 2008.

[13] A. Daraghmeh, C. Hartmann, and N. Qatanani, "Balanced model reduction of linear systems with nonzero initial conditions: Singular perturbation approximation," *Applied Mathematics and Computation*, vol. 353, pp. 295–307, 2019.

[14] Y. Liu and B. D. Anderson, "Singular perturbation approximation of balanced systems," *International Journal of Control*, vol. 50, no. 4, pp. 1379–1405, 1989.

[15] O. Ajala, A. D. Domínguez-García, and P. W. Sauer, "A hierarchy of models for inverter-based microgrids," in *Energy Markets and Responsive Grids*. Springer, 2018, pp. 307–332.

[16] J. Chow, J. Winkelman, M. Pai, and P. W. Sauer, "Singular perturbation analysis of large-scale power systems," *International Journal of Electrical Power & Energy Systems*, vol. 12, no. 2, pp. 117–126, 1990.

[17] H. Khalil, *Nonlinear Systems*. Prentice Hall; Third edition, 2002.

[18] P. Kokotovic, H. K. Khali, and J. O'reilly, *Singular perturbation methods in control: analysis and design*. Siam, 1999, vol. 25.

[19] D. Del Vecchio and J. J. E. Slotine, "A contraction theory approach to singularly perturbed systems," *IEEE Trans. on Auto. Control*, vol. 58, no. 3, pp. 752–757, 2013.

[20] S. Zhai, "Bounded synchronisation of singularly perturbed complex network with an application to power systems," *IET Control Theory Applications*, vol. 8, pp. 61–66(5), January 2014.

[21] M. M. Rayguru and I. N. Kar, "Contraction-based stabilisation of nonlinear singularly perturbed systems and application to high gain feedback," *International Journal of Control*, 2016.

[22] M. M. Rayguru and I. N. Kar, "High gain observer based saturated controller for feedback linearizable system," *IEEE Transactions on Circuits and Systems II: Express Briefs*, pp. 1–1, Jan. 2020.

[23] N. Pogaku, M. Prodanovic, and T. C. Green, "Modeling, analysis and testing of autonomous operation of an inverter-based microgrid," *IEEE Transactions on Power Electronics*, vol. 22, no. 2, pp. 613–625, March 2007.

[24] M. Safonov, R. Chiang, and D. Limebeer, "Optimal hankel model reduction for nonminimal systems," *IEEE Transactions on Automatic Control*, vol. 35, no. 4, pp. 496–502, 1990.

[25] M. G. Safonov and R. Y. Chiang, "Model reduction for robust control: A schur relative-error method," in *1988 American Control Conference*, 1988, pp. 1685–1690.

[26] W. Lohmiller and J.-J. E. Slotine, "On contraction analysis for non-linear systems," *Automatica*, vol. 34, no. 6, pp. 683–696, June 1998.

[27] W. Wang and J.-J. E. Slotine, "On partial contraction analysis for coupled nonlinear oscillators," *Biological cybernetics*, vol. 92, no. 1, pp. 38–53, 2005.

[28] D. Del Vecchio and J.-J. Slotine, "A contraction theory approach to singularly perturbed systems with application to retroactivity attenuation," in *Decision and Control and European Control Conference (CDC-ECC), 2011 50th IEEE Conference on*, March 2013, pp. 5831–5836.

[29] M. M. Rayguru and I. N. Kar, "Contraction theory approach to disturbance observer based filtered backstepping design," *ASME. J. Dyn. Sys., Meas., Control.l*, 2019.